Inactivation of mouse *Hus1* results in genomic instability and impaired responses to genotoxic stress

Robert S. Weiss, Tamar Enoch, and Philip Leder[1,2]

Department of Genetics and [1]Howard Hughes Medical Institute, Harvard Medical School, Boston, Massachusetts 02115 USA

The eukaryotic cell cycle is overseen by regulatory mechanisms, termed checkpoints, that respond to DNA damage, mitotic spindle defects, and errors in the ordering of cell cycle events. The DNA replication and DNA damage cell cycle checkpoints of the fission yeast *Schizosaccharomyces pombe* require the *hus1*$^+$ (*hydroxyurea sensitive*) gene. To determine the role of the mouse homolog of *hus1*$^+$ in murine development and cell cycle checkpoint function, we produced a targeted disruption of mouse *Hus1*. Inactivation of *Hus1* results in mid-gestational embryonic lethality due to widespread apoptosis and defective development of essential extra-embryonic tissues. DNA damage-inducible genes are up-regulated in *Hus1*-deficient embryos, and primary cells from *Hus1*-null embryos contain increased spontaneous chromosomal abnormalities, suggesting that loss of *Hus1* leads to an accumulation of genome damage. Embryonic fibroblasts lacking *Hus1* fail to proliferate in vitro, but inactivation of *p21* allows for the continued growth of *Hus1*-deficient cells. *Hus1*$^{-/-}$*p21*$^{-/-}$ cells display a unique profile of significantly heightened sensitivity to hydroxyurea, a DNA replication inhibitor, and ultraviolet light, but only slightly increased sensitivity to ionizing radiation. Taken together, these results indicate that mouse *Hus1* functions in the maintenance of genomic stability and additionally identify an evolutionarily-conserved role for *Hus1* in mediating cellular responses to genotoxins.

[*Key Words*: Apoptosis; cell cycle checkpoints; genomic instability; DNA damage]

Received May 4, 2000; revised version accepted June 15, 2000.

Cell cycle checkpoints are surveillance mechanisms that monitor the cell cycle and protect genome integrity by inducing cell cycle arrest or programmed cell death in response to DNA damage, mitotic spindle defects, or errors in the ordering of cell cycle events (Hartwell and Weinert 1989; Elledge 1996). Among these regulatory pathways are the DNA replication checkpoint, which couples mitosis to the completion of DNA replication, and the DNA damage checkpoint, which promotes the repair of DNA lesions before DNA replication or cell division. In addition to overseeing progression of the mitotic cell cycle, checkpoint proteins also act to maintain telomeres (Dahlen et al. 1998; Ahmed and Hodgkin 2000), to monitor meiosis (for review, see Page and Orr-Weaver 1997), and to regulate dNTP biosynthesis and maintain the cellular capacity for DNA synthesis (Desany et al. 1998; Zhao et al. 1998). Defects in checkpoint pathways can result in cell death or genomic instability. In mammals, genomic instability is thought to promote tumorigenesis (Hartwell and Kastan 1994; Lengauer et al. 1998), and mutations in the checkpoint genes *p53* (for review, see Levine 1997), *ATM* (for review, see Rotman and Shiloh 1999), and *hCHK2* (Bell et al. 1999) are associated with familial cancer syndromes. In addition, cellular responses to anticancer drugs, many of which act by damaging DNA or inhibiting DNA replication, may depend largely on the activity of cell cycle checkpoints (Hartwell and Kastan 1994).

Recent studies indicate that several features of cell cycle checkpoints are conserved throughout evolution. As a result, knowledge of cell cycle checkpoints in the budding yeast *Saccharomyces cerevisiae* and the fission yeast *Schizosaccharomyces pombe* provides a framework for developing a further understanding of checkpoint pathways in higher eukaryotes. In fission yeast six non-essential genes (*hus1*$^+$, *rad1*$^+$, *rad3*$^+$, *rad9*$^+$, *rad17*$^+$, and *rad26*$^+$), known as the *checkpoint rad* genes, are required for both the DNA replication and DNA damage checkpoints (Al-Khodairy and Carr 1992; Enoch et al. 1992; Rowley et al. 1992; Al-Khodairy et al. 1994). With the possible exception of *rad26*$^+$, each of the *checkpoint rad* genes is represented in mammals by a closely related homolog (for review, see Caspari and Carr 1999; Dasika et al. 1999). Evidence that this sequence homology reflects conserved protein function is provided by the

[2]**Corresponding author.**
E-MAIL leder@rascal.med.harvard.edu; FAX (617) 432-7663.

rad3$^+$-related gene *ATM*, which encodes a bona fide mammalian checkpoint protein. In addition to the *checkpoint rad* genes, other fission yeast genes that function in checkpoint responses, such as *chk1*$^+$ and *cds1*$^+$, also appear to be retained in higher eukaryotes (for review, see Caspari and Carr 1999; Dasika et al. 1999). Taken together, these evolutionarily-conserved checkpoint genes may represent a core checkpoint apparatus, analysis of which will likely provide considerable insight into mammalian DNA damage responses.

Fission yeast *hus1*$^+$ (*hydroxyurea sensitive*) was originally identified in a screen for genes that, when inactivated, conferred sensitivity to the DNA replication inhibitor hydroxyurea (HU) (Enoch et al. 1992). Fission yeast lacking *hus1*$^+$ appear normal under standard growth conditions, but fail to arrest the cell cycle after DNA damage or blockage of DNA synthesis (Enoch et al. 1992; Kostrub et al. 1997). Instead, *hus1*$^-$ strains proceed into mitosis with damaged or incompletely replicated genomes. In addition, *hus1*$^+$ plays a role in the poorly understood process of recovery from S-phase arrest, as HU-treated *hus1*$^-$ yeast become irreversibly damaged during interphase, before undergoing premature cell division (Enoch et al. 1992). Although the Hus1p polypeptide lacks domains that might indicate its biochemical function, sequence analyses suggest that Hus1p may be structurally similar to the DNA sliding clamp protein PCNA, which forms a trimer that encircles DNA (Aravind et al. 1999; Caspari et al. 2000). Hus1p is phosphorylated after DNA damage, and this modification requires the other *checkpoint rad* proteins, including the ATM-related kinase Rad3p (Kostrub et al. 1998). In addition, Hus1p physically associates with two other checkpoint polypeptides, Rad1p and Rad9p (Kostrub et al. 1998; Caspari et al. 2000).

Homologs of *hus1*$^+$ have been identified in a number of higher eukaryotes, including *Mus musculus* and *Homo sapiens* (Dean et al. 1998; Kostrub et al. 1998). The mammalian Hus1 proteins are similar in length to Hus1p and share ~30% amino acid identity with the *S. pombe* protein. The notion that these homologs are functionally equivalent to their fission yeast counterpart is strengthened by the finding that the human HUS1 protein interacts with human RAD1 and RAD9 polypeptides (St. Onge et al. 1999; Volkmer and Karnitz 1999). Mouse *Hus1* is a single copy gene located at the proximal end of chromosome 11 (Weiss et al. 1999). It is expressed throughout embryonic development and displays a ubiquitous expression pattern in adult tissues. To determine the role of *Hus1* in murine development and cell cycle checkpoint function, we produced a targeted disruption of *Hus1*. Here, we report that *Hus1* inactivation causes mid-gestational embryonic lethality. *Hus1*-null embryos show transcriptional induction of DNA damage-responsive genes and yield cells that contain increased spontaneous chromosomal abnormalities, suggesting that *Hus1* is required for the maintenance of genomic stability. In addition, analysis of *Hus1*-deficient fibroblast cultures indicates that mouse *Hus1*, like *S. pombe hus1*$^+$, has a role in cellular responses to genotoxic stress.

Results

Hus1-*deficiency results in mid-gestational embryonic lethality*

Mouse *Hus1* was disrupted by homologous recombination in embryonic stem (ES) cells using a targeting vector in which 1 kb of genomic sequence from the *Hus1* locus was deleted (Fig. 1A). Because the deleted region included *Hus1* exon one and the translation initiation codon, homologous recombination of the targeting construct was predicted to produce a null *Hus1* allele. The targeting construct was electroporated into TC-1 ES cells (Deng et al. 1996) and, of 120 G418- and FIAU-resistant clones screened by Southern blot hybridization, eight were found to be correctly targeted (Fig. 1B). Five of the targeted ES cell clones were micro-injected into donor blastocysts, and chimeric males derived from three of the clones transmitted the targeted allele through the germline when mated with 129S6 and Black Swiss females. Mice heterozygous for the targeted allele (*Hus1*$^{+/-}$) were normal and fertile, and no overt phenotypes have been observed in *Hus1*$^{+/-}$ mice at up to one year of age.

Hus1$^{+/-}$ mice were intercrossed in order to produce *Hus1*$^{-/-}$ mice. However, no nullizygous mice were detected among 243 offspring, indicating that loss of *Hus1* caused recessive embryonic lethality (Table 1). To characterize the timing and nature of the embryonic lethality, we analyzed the morphology of embryos from timed *Hus1* heterozygote intercrosses at different stages of gestation. Embryos were genotyped by PCR (Fig. 1C). At 7.5 dpc (days post coitum) *Hus1*$^{-/-}$ embryos appeared grossly normal but were on average slightly smaller than *Hus1*$^{+/+}$ or *Hus1*$^{+/-}$ littermates (Table 1; Fig. 2A). Examination of histological sections from 7.5 dpc *Hus1* embryos confirmed these observations and additionally revealed that *Hus1*$^{-/-}$ embryos gastrulated normally (data not shown). By 8.5 dpc, *Hus1*$^{-/-}$ embryos showed atypical small size and occasional morphological defects (Table 1; Fig. 2B). In addition, *Hus1*-deficient embryos at 8.5 dpc were developmentally delayed, possessing fewer somites than normal embryos and failing to initiate axial rotation. At 9.5 dpc, *Hus1*$^{-/-}$ embryos were invariably abnormal, showing small size, severe developmental delay, and numerous morphological abnormalities (Table 1; Fig. 2C–E). *Hus1*-null embryos at 9.5 dpc failed to undergo axial rotation, whereas normal embryos had completely turned by this time. The posterior of *Hus1*$^{-/-}$ embryos was severely underdeveloped and limb bud formation could not be detected. *Hus1*$^{-/-}$ embryos had eight to 13 somites at this stage, compared to the 20–24 somites of normal embryos, and the somites of *Hus1*-null embryos often appeared misshapen (Fig. 2C). The neural tube of *Hus1*$^{-/-}$ embryos showed extensive kinking (Fig. 2C), and the head folds of nullizygous embryos usually failed to close (Fig. 2C,E), although a few *Hus1*$^{-/-}$ embryos showed more advanced development of cranial structures (Fig. 2D). In 17% (4 of 23) of *Hus1*-null embryos, the allantois failed to fuse to the chorion by 9.5 dpc and instead appeared as a swollen, bulbous structure

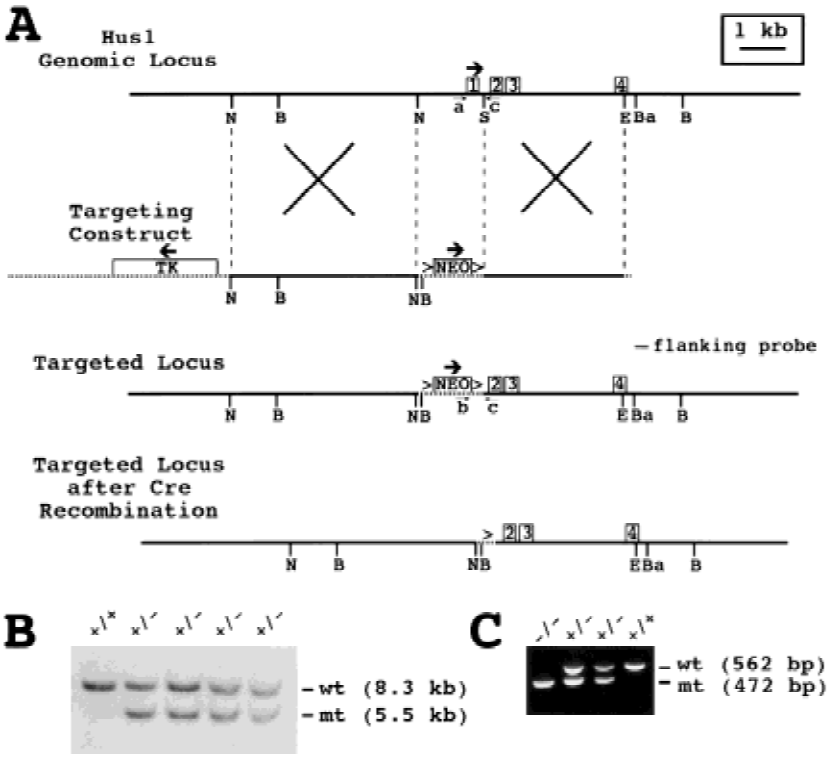

Figure 1. Targeted disruption of the mouse *Hus1* gene. (*A*) Restriction maps of the *Hus1* genomic locus, targeting construct, targeted locus, and targeted locus following *cre*-mediated recombination. The first four *Hus1* exons are shown as boxes. Vector-derived sequences are shown as stippled lines, and thick arrows indicate the direction of transcription for the *Hus1*, neomycin resistance (*Neo*), and thymidine kinase (*Tk*) genes. LoxP sites are represented by the (>) symbols. The positions of the flanking probe and PCR primers a, b, and c used for genotyping are indicated. Homologous recombination of the targeting construct is depicted by the large Xs. (B) *Bgl*II, (Ba) *Bam*HI, (E) *Eco*RV, (N) *Nhe*I, (S) *Sma*I. (*B*) Southern blot analysis of ES cell genomic DNA. Genomic DNA from wild-type TC-1 cells (+/+) or four independent targeted ES cell clones (+/−) was digested with *Bgl*I and hybridized with the flanking probe. The positions of the bands corresponding to the wild-type (wt) and targeted mutant (mt) *Hus1* alleles are indicated. (*C*) Representative PCR analysis of yolk sac genomic DNA obtained from progeny of a *Hus1* heterozygote intercross using the primers shown in *A*. The positions of PCR products from the wild-type (wt) and targeted mutant (mt) *Hus1* alleles are indicated.

at the posterior of the embryo (Fig. 2E), a phenotype also observed in irradiated rat embryos (Kuznetsova 1957; Walshtrem 1960). Approximately one-half of *Hus1*$^{-/-}$ embryos possessed a beating heart at 9.5 dpc, but only a single live *Hus1*$^{-/-}$ embryo was identified at 10.5 dpc. No additional development of *Hus1*$^{-/-}$ embryos beyond that observed at 9.5 dpc was detected at 10.5 dpc, and intact *Hus1*$^{-/-}$ embryos were not detected at latter stages of gestation (Table 1). Similar results were obtained from the analysis of mice derived from three independent ES cell clones. In a pure 129S6 genetic background, the phenotype of *Hus1*$^{-/-}$ embryos was similar but more severe than that described above for the mixed (129S6 × Black Swiss) background, resulting in the death of all *Hus1*$^{-/-}$ embryos by 9.5 dpc (data not shown). In addition, the *Hus1*$^{-/-}$ phenotype was unchanged following *cre*-mediated recombination at the targeted allele (Fig. 1A; data not shown), indicating that embryonic lethality did not result from interference with neighboring gene function by the *Neo* cassette.

Table 1. *Genotype and phenotype analysis of offspring from* Hus1 *heterozygote matings*[a]

	Genotype			
Stage	+/+	+/−	−/−	Resorptions
7.5 dpc	23	38	18	1
8.5 dpc	9	24 (1A)[b]	16 (15A)	1
9.5 dpc	21	35 (1A)	23 (23A)	4
10.5 dpc	16 (1A)	28 (1A)	9 (9A)	7
11.5–13.5 dpc	10	25	0	16
Weanling	83	160	0	—

[a]For each developmental stage, the number of embryos of each genotype and the number of resorptions is indicated. The number of phenotypically abnormal embryos is noted in parentheses.
[b](A) Abnormal embryo defined by small size, developmental delay, or morphological defects; see text for detailed description of mutant embryo phenotypes.

Extra-embryonic defects in Hus1*-null embryos*

In several mouse models, the occurrence of embryonic lethality between 10.5 and 12.5 dpc is due to defective development of the yolk sac and/or placenta, which become essential at this stage of gestation (for review, see Copp 1995). Because loss of *Hus1* caused a similar mid-gestational embryonic lethality, we investigated the development of extra-embryonic tissues in *Hus1*-null embryos. The yolk sac transports nutrients and gases from the surrounding maternal deciduum to the embryo (for review, see Cross et al. 1994; Rinkenberger et al. 1997). By gross inspection, the yolk sacs of 9.5 dpc *Hus1*$^{+/+}$ and *Hus1*$^{+/-}$ embryos were well-vascularized and contained numerous blood-filled vitillene vessels (Fig. 3A). In contrast, the yolk sacs of *Hus1*$^{-/-}$ embryos appeared thin and fragile, and lacked prominent vasculature, although some blood cells could be detected (Fig. 3B). These observations prompted a histological analysis of yolk sac

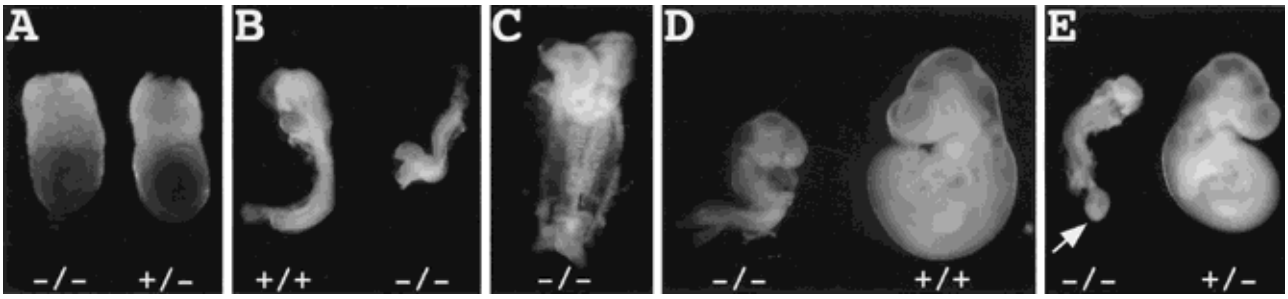

Figure 2. Morphology of *Hus1* embryos. Embryos from timed *Hus1* heterozygote intercrosses were photographed at the time of dissection and genotyped thereafter. (*A*) 7.5 dpc, (*B*) 8.5 dpc, (*C–E*) 9.5 dpc. Arrow in *E* indicates hydropic allantois.

development in *Hus1* embryos. The yolk sac circulation derives from extra-embryonic mesodermal aggregates termed blood islands (for review, see Cross et al. 1994; Rinkenberger et al. 1997). Blood islands formed by 8.0 dpc in *Hus1* embryos of all genotypes, but the blood islands of *Hus1*$^{-/-}$ embryos contained cells with abnormal pyknotic nuclei which were not observed in blood islands from *Hus1*$^{+/+}$ or *Hus1*$^{+/-}$ embryos (Fig. 3C,D). Furthermore, whereas the blood islands of *Hus1*$^{+/+}$ and *Hus1*$^{+/-}$ embryos gave rise to numerous vessels filled with primitive, nucleated blood cells by 9.5 dpc (Fig. 3E), blood cells were scarce in sections of yolk sac from *Hus1*$^{-/-}$ littermates and atypical cells with pyknotic nuclei were apparent (Fig. 3F,G).

Development of the chorioallantoic placenta was also examined. As described earlier, the allantois failed to fuse with the chorion in a subset of *Hus1*-deficient embryos. However, the morphology of *Hus1*$^{-/-}$ embryos was the same regardless of whether chorioallantoic fusion had occurred, suggesting that the fusion events that did happen were not productive. When chorioallantoic fusion did occur, embryonic blood cells were nevertheless absent from the primitive umbilicus of *Hus1*$^{-/-}$ embryos, unlike *Hus1*$^{+/+}$ or *Hus1*$^{+/-}$ embryos (data not shown). In addition, although all four embryonic layers of the placenta were present in *Hus1*$^{-/-}$ embryos, the labyrinthine layer was abnormally compact and avascular (Fig. 3H,I). Furthermore, numerous apoptotic cells were detected throughout the chorionic plate, and embryonic blood cells were notably absent from this region. These data suggest that the death of *Hus1*$^{-/-}$ embryos is due in part to defective development of essential extra-embryonic tissues.

Increased apoptosis but normal cell proliferation in Hus1$^{-/-}$ *embryos*

The two primary cellular responses to genotoxic stress in mammals are apoptosis and cell cycle arrest. We reasoned that, in the absence of *Hus1*, these processes might be deregulated and that increased apoptosis or reduced cell proliferation could account for the small size and developmental delay observed in *Hus1*$^{-/-}$ embryos. Evaluations of histological sections from *Hus1* embryos indicated that *Hus1*$^{-/-}$ embryos contained increased numbers of cells with pyknotic nuclei, a characteristic of apoptotic cells. Therefore, the occurrence of apoptosis in embryo sections was assessed more rigorously by TUNEL (TdT-mediated dUTP nick end labeling) staining, a method for detecting apoptosis based on the presence of fragmented DNA in apoptotic cells. As expected, few TUNEL-positive cells were observed in *Hus1*$^{+/+}$ and *Hus1*$^{+/-}$ embryos (Fig. 4A–D), and none were detected in control sections on which mock TUNEL staining was performed without TdT enzyme (data not shown). In contrast, TUNEL staining of *Hus1*$^{-/-}$ embryo sections at 7.5 dpc identified multiple apoptotic cells within the amniotic cavity and scattered throughout the embryo (Fig. 4F). Increased numbers of TUNEL-positive apoptotic cells were also observed in *Hus1*$^{-/-}$ embryos at 8.0 and 8.5 dpc (Fig. 4G–I). Cell death was widespread in *Hus1*$^{-/-}$ embryos and appeared to occur in all cell types. Quantitation of TUNEL-positive cells in embryonic ectoderm revealed an ~5-fold elevation in apoptosis in *Hus1*-deficient embryos at 7.5, 8.0, and 8.5 dpc.

Further examination of histological sections from *Hus1* embryos indicated that the mitotic index of *Hus1*$^{-/-}$ embryos was normal (data not shown). To confirm that cell proliferation was unaffected by loss of *Hus1*, we examined the ability of *Hus1* embryos to incorporate BrdU, an indication of DNA synthesis and thus a marker for S-phase of the cell cycle. Embryos were labeled with BrdU in utero, sectioned, and stained with an anti-BrdU monoclonal antibody. Normal embryos at 7.5 dpc are characterized by rapid cell proliferation, and ~85% of cells in the epiblast of *Hus1*$^{+/+}$ or *Hus1*$^{+/-}$ embryos were BrdU-positive (Fig. 4E). A similar frequency of BrdU incorporation was detected in *Hus1*$^{-/-}$ embryos (Fig. 4J). Furthermore, regardless of genotype, ~75% of embryonic ectodermal cells from 8.5 dpc embryos stained positive for BrdU incorporation (data not shown). Thus, cells of *Hus1*-deficient embryos appear to proliferate normally but undergo apoptosis at a relatively high frequency.

Increased expression of DNA damage-responsive genes in Hus1*-deficient embryos*

Given the role of cell cycle checkpoints in maintaining the integrity of the genome, genomic instability and DNA damage accumulation were possible consequences of *Hus1* inactivation. As a readout for the presence of

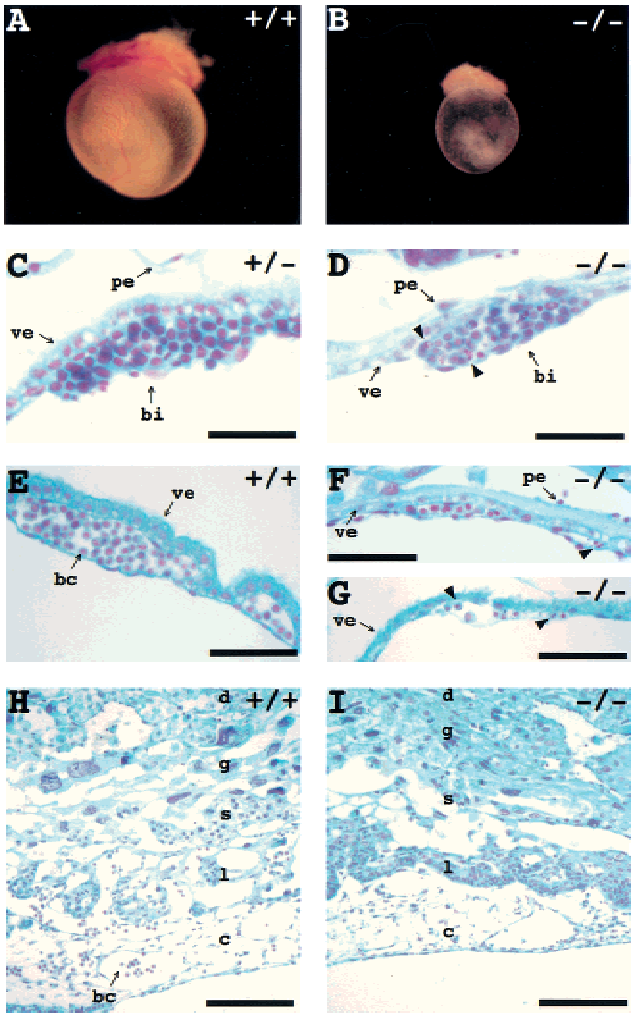

Figure 3. Abnormal development of yolk sac and placenta in *Hus1*$^{-/-}$ embryos. (*A*,*B*) *Hus1* embryos at 9.5 dpc were photographed following removal of deciduum, trophoblast giant cells, and Reichert's membrane. (*C*–*I*) Sections of embryos from timed *Hus1* heterozygote intercrosses were stained by the Feulgen method. (*C*,*D*) 8.5 dpc blood islands; (*E*–*G*) 9.5 dpc yolk sacs; (*H*,*I*) 9.5 dpc placentas. Arrowheads indicate some of the cells with pyknotic or otherwise abnormal nuclei. Abbreviations: (bc) blood cell, (bi) blood island, (c) chorionic plate, (d) maternal decidua, (g) trophoblast giant cell layer, (l) labyrinthine layer, (pe) parietal endoderm, (s) spongiotrophoblast layer, (ve) visceral endoderm. Size bars: (*C*,*D*) 31 μm; (*E*–*G*) 62.5 μm; (*H*,*I*) 125 μm.

DNA damage in *Hus1* embryos, the expression levels of *p21* and other DNA damage-responsive genes were examined by Northern blot hybridization. RNA was prepared from individual *Hus1* embryos at 8.5 dpc, a stage at which *Hus1*$^{-/-}$ embryos were consistently abnormal morphologically but did not show severe defects that might indirectly affect the expression of many genes. Contaminating genomic DNA in the RNA samples permitted genotyping by PCR (data not shown). The RNAs were first hybridized to a probe encompassing the entire *Hus1* open reading frame to verify the genotypes obtained by PCR and to determine whether any *Hus1* transcripts were produced from the targeted allele. Importantly, no *Hus1* transcripts were detected in *Hus1*$^{-/-}$ embryos, confirming that the targeted disruption of *Hus1* resulted in a null allele (Fig. 5A). As expected, reduced levels of *Hus1* mRNA were detected in *Hus1*$^{+/-}$ embryos relative to *Hus1*$^{+/+}$ embryos.

The same Northern blot was then sequentially hybridized to a series of cDNA probes for genes involved in cellular DNA damage responses. Because less total RNA was obtained from the undersized *Hus1*$^{-/-}$ embryos, results were quantitated on a PhosphorImager and values were normalized based on results for the loading control, *Gapdh* (Fig. 5B). First to be assessed was the *p53*-regulated, DNA damage-inducible gene *p21* (for review, see Ko and Prives 1996). A striking increase in *p21* mRNA was detected in all *Hus1*$^{-/-}$ embryos (mean induction of 9.9-fold in *Hus1*$^{-/-}$ versus *Hus1*$^{+/+}$ and *Hus1*$^{+/-}$ embryos). The expression levels of *Mdm2* and *Bax*, two additional *p53*-regulated genes that are induced following DNA damage (for review, see Ko and Prives 1996), were also elevated in the absence of *Hus1* (mean induction of 2.6- and 2.1-fold for *Mdm2* and *Bax*, respectively). Also examined was the expression of *Gadd34*, a DNA damage-responsive gene that is regulated in a *p53*-independent manner (Hollander et al. 1997). A modest increase in *Gadd34* expression (mean induction of 2.1-fold) was detected in *Hus1*-null embryos. To determine the specificity of the changes in gene expression observed in *Hus1*$^{-/-}$ embryos, we examined the expression of *Rad1*, the human homolog of which encodes a HUS1-interacting protein (St. Onge et al. 1999; Volkmer and Karnitz 1999) that is not induced by DNA damage (Freire et al. 1998; Parker et al. 1998). Consistent with the observation that fission yeast lacking *hus1*$^{+}$ show no alterations in *rad1*$^{+}$ expression (Kostrub et al. 1998), *Rad1* expression was found to be essentially unchanged in *Hus1*$^{-/-}$ embryos (mean induction of 1.2-fold). Thus, loss of *Hus1* specifically results in transcriptional upregulation of *p21* and, to lesser extents, other DNA damage-inducible genes.

Chromosomal abnormalities in Hus1$^{-/-}$ *embryos*

The elevated expression of *p21* and other DNA damage-responsive genes observed in *Hus1*$^{-/-}$ embryos suggested that *Hus1*-deficient embryos might contain increased DNA damage. To directly assess genome damage in *Hus1*-null embryos, we examined the frequency of chromosomal abnormalities in metaphase spreads prepared from primary *Hus1* embryo cultures. A total of 9 *Hus1*$^{+/+}$, 26 *Hus1*$^{+/-}$, and 14 *Hus1*$^{-/-}$ embryos, from five litters, were assessed. Representative metaphases are shown in Figure 6. A significant increase in chromosomal abnormalities was detected in *Hus1*$^{-/-}$ embryos, as 55% (45 of 82) of metaphases from *Hus1*$^{-/-}$ embryos contained at least one chromosomal abnormality, compared to only 19% (24 of 130) of metaphases from *Hus1*$^{+/+}$ or *Hus1*$^{+/-}$ embryos ($\chi^2 = 30.37$, $P < 0.001$). Chromatid breaks were the most common abnormality in *Hus1*$^{-/-}$ embryos, and this type of aberration was observed in 43

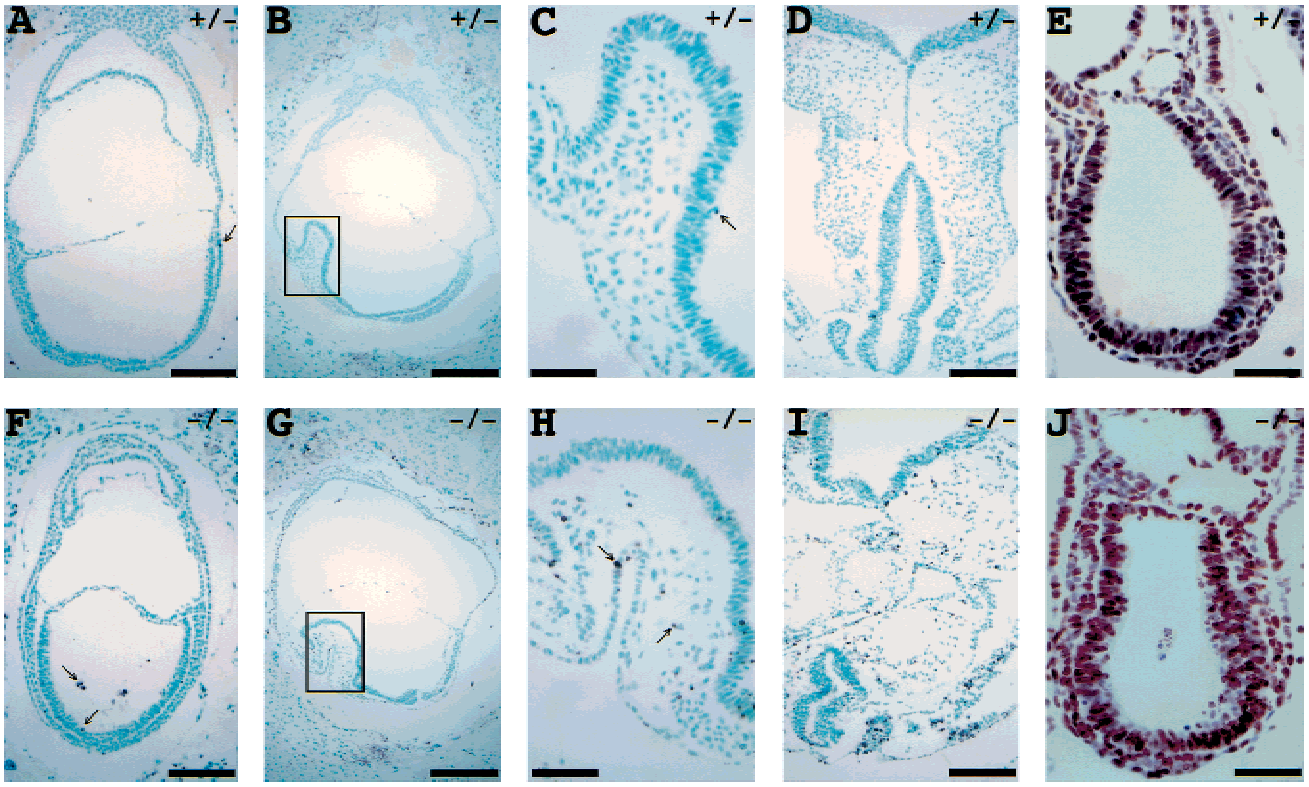

Figure 4. Increased apoptosis but normal cell proliferation in *Hus1*$^{-/-}$ embryos. (*A–D*,*F–I*) Sections of *Hus1* embryos were stained by the TUNEL method. (*A*,*F*) 7.5 dpc, (*B*,*G*) 8.0 dpc, (*C*,*H*) higher magnification view of boxed region in *B* and *G*, (*D*,*I*) 8.5 dpc. Arrows in *A*, *C*, *F*, and *H* indicate some of the TUNEL-positive apoptotic cells, which are darkly-stained in contrast to the methyl green counterstain. (*E*,*J*) Sections of BrdU-labeled *Hus1* embryos at 7.5 dpc were stained with an anti-BrdU antibody. BrdU-positive cells are darkly-stained in contrast to the hematoxylin (blue) counterstain. Size bars: (*A*,*D*,*F*,*I*) 125 μm; (*B*,*G*) 250 μm; (*C*,*E*,*H*,*J*) 62.5 μm.

of 82 *Hus1*$^{-/-}$ metaphases. Also detected were chromatid gaps (4 of 82), terminal deletions (5 of 82), acentric fragments (4 of 82), and chromatid exchanges (11 of 82). A similar distribution of abnormalities was observed at reduced frequency in *Hus1*$^{+/+}$ and *Hus1*$^{+/-}$ embryos, and included chromatid breaks (21 of 130), chromatid gaps (2 of 130), acentric fragments (1 of 130), and chromatid exchanges (3 of 130). More striking than the increased occurrence of abnormal metaphases in *Hus1*$^{-/-}$ cells was the frequency of metaphases containing multiple chromosomal abnormalities. Forty-four percent (36 of 82) of metaphases from *Hus1*$^{-/-}$ embryos contained more than one aberration and 27% (22 of 82) contained greater than five, whereas only 4% (5 of 130) of metaphases from *Hus1*$^{+/+}$ or *Hus1*$^{+/-}$ embryos contained more than one abnormality and none had greater than four abnormalities. Moreover, some metaphases from *Hus1*$^{-/-}$ cells contained such extensive chromosome damage that the abnormalities could not be enumerated (Fig. 6C). These data suggest an important role for *Hus1* in the maintenance of genomic stability.

Increased sensitivity of Hus1*-deficient cells to genotoxic stress*

To facilitate additional studies of *Hus1* cellular functions, we attempted to culture mouse embryonic fibroblasts (MEFs) from 9.5 dpc *Hus1* embryos. Whereas *Hus1*$^{+/+}$ and *Hus1*$^{+/-}$ MEF cultures grew well and could be serially passaged, *Hus1*$^{-/-}$ MEFs failed to proliferate (data not shown). In light of the increased chromosomal abnormalities in primary *Hus1*-null cells, it seemed plausible that spontaneous genome damage in *Hus1*$^{-/-}$ MEFs might trigger a *Hus1*-independent checkpoint, resulting in cell cycle arrest. A likely candidate for enforcing such a growth arrest was *p21*, given its increased expression in *Hus1*-null embryos. Therefore, the targeted *Hus1* allele was bred onto a *p21*$^{-/-}$ background, and MEFs were generated from *Hus1*$^{+/-}$*p21*$^{-/-}$ intercrosses at 9.5 dpc to determine if deletion of *p21* might enable *Hus1*-deficient cells to continue proliferating. Whereas *Hus1*$^{-/-}$ MEFs failed to proliferate under the same conditions, cells from three of 13 *Hus1*$^{-/-}$*p21*$^{-/-}$ embryos placed into culture continued to divide and could be continuously passaged. It is unclear whether the low efficiency of establishing *Hus1*$^{-/-}$*p21*$^{-/-}$ cultures is due to a requirement for additional genetic changes or is a reflection of technical difficulties associated with culturing abnormal embryos at an early developmental stage. Northern blot analyses confirmed that the *Hus1*$^{-/-}$*p21*$^{-/-}$ MEFs did not contain wild-type *Hus1* transcripts but revealed aberrant *Hus1* transcripts that were not detected in *Hus1*$^{-/-}$ embryos (data not shown). Because the targeted allele lacks *Hus1* exon one and the

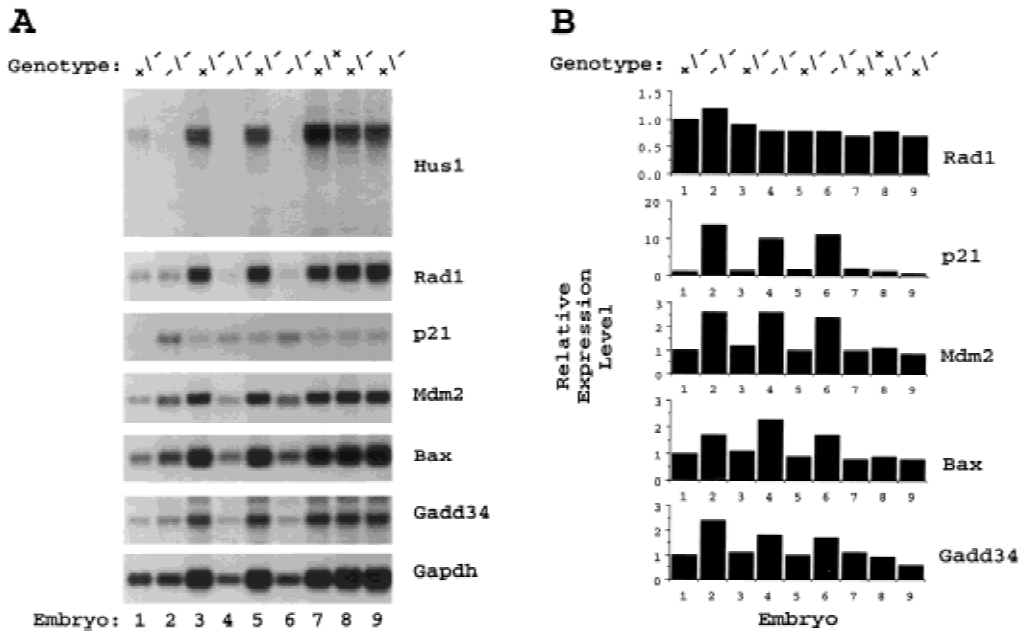

Figure 5. Lack of detectable *Hus1* transcripts but elevated expression of DNA damage-inducible genes in *Hus1*$^{-/-}$ embryos. (*A*) Northern blot analysis of 8.5 dpc embryos from a timed *Hus1* heterozygote intercross. Total RNA was prepared from individual embryos and subjected to Northern blot hybridization with the indicated ^{32}P-labeled cDNA probes. Note that *Hus1*$^{-/-}$ embryos are smaller than normal embryos at 8.5 dpc and therefore appear to be under-loaded. A portion of the RNA from embryo number one was lost during sample preparation and thus approximately equal amounts of RNA were obtained from this *Hus1*$^{+/-}$ embryo and the *Hus1*$^{-/-}$ embryos. (*B*) Quantitative analysis of gene expression levels. Radioactive signal intensity was quantitated with a PhosphorImager. Values were normalized based on results for the loading control *Gapdh*, and for each cDNA probe the expression level in each embryo is shown relative to the signal for embryo one, which was assigned an arbitrary expression level of one.

translation initiation codon, it is unlikely that these mRNAs give rise to functional Hus1 protein, although we cannot rule out the possibility that truncated Hus1 proteins are produced. The *Hus1*$^{-/-}$*p21*$^{-/-}$ cells showed growth rates similar to those of *Hus1*$^{+/+}$*p21*$^{-/-}$ cells, despite the presence of increased chromosomal abnormalities (data not shown).

Fission yeast lacking *hus1*$^{+}$ are highly sensitive to DNA replication inhibitors as well as various DNA damaging agents, including ultraviolet light (UV) and the radiomimetic drug bleomycin (Enoch et al. 1992; Kostrub et al. 1998). To test whether mouse *Hus1* was likewise required for proper cellular responses to genotoxic stress, we examined the viability of *Hus1*$^{-/-}$*p21*$^{-/-}$ and

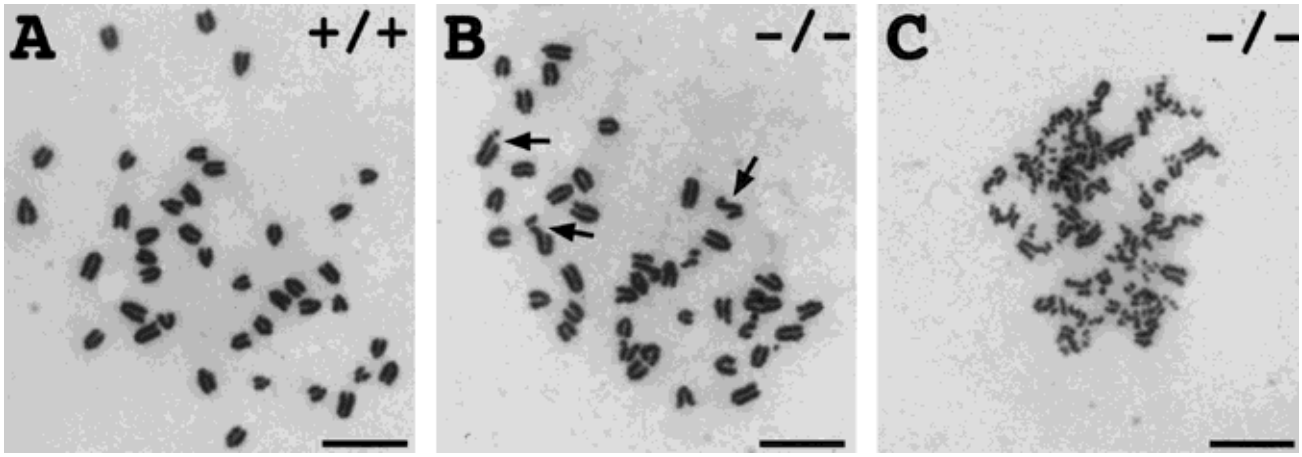

Figure 6. Chromosomal abnormalities in primary cultures of *Hus1*$^{-/-}$ embryos. Metaphase spreads were prepared from primary cultures of 9.5 dpc *Hus1* embryos and stained with Giemsa. Shown are: (*A*) A normal *Hus1*$^{+/+}$ metaphase, (*B*) a *Hus1*$^{-/-}$ metaphase containing multiple chromatid breaks, and (*C*) a *Hus1*$^{-/-}$ metaphase with extensive chromosome damage. Arrows in *B* indicate some of the chromatid breaks. Size bar: 12.5 μm.

Hus1$^{+/+}$*p21*$^{-/-}$ cells after treatment with increasing doses of HU, UV, and ionizing radiation (IR). *Hus1*$^{-/-}$ *p21*$^{-/-}$ MEFs were 5- to 10-fold more sensitive to HU than *Hus1*$^{+/+}$*p21*$^{-/-}$ cells, suggesting that *Hus1* participates in cellular responses to DNA replication blocks (Fig. 7A). The *Hus1*$^{-/-}$ *p21*$^{-/-}$ cells also showed an increased sensitivity to UV (Fig. 7B). Surprisingly, however, the *Hus1*$^{-/-}$*p21*$^{-/-}$ cells did not display a similarly heightened sensitivity to IR. In some experiments, the *Hus1*$^{-/-}$*p21*$^{-/-}$ cells showed a less than twofold increase in sensitivity to IR (Fig. 7C), whereas in other experiments even this slight difference in IR sensitivity was not observed. Therefore, we conclude that loss of *Hus1* results in significantly increased sensitivity to HU and UV, but has a relatively minor effect on IR sensitivity.

Although three independent *Hus1*$^{-/-}$*p21*$^{-/-}$ cultures gave results similar to those shown in Figure 7, it was possible that these findings were affected by secondary mutations that might have arisen during the culturing of *Hus1*–null cells. To confirm that the increased sensitivity of *Hus1*$^{-/-}$*p21*$^{-/-}$ cells to genotoxins was due to the absence of *Hus1*, we tested whether restoring *Hus1* expression would rescue the UV sensitivity of *Hus1*$^{-/-}$*p21*$^{-/-}$ cells. *Hus1*$^{-/-}$*p21*$^{-/-}$ and control *Hus1*$^{+/+}$ *p21*$^{-/-}$ cells were stably transfected with either an expression plasmid encoding *Hus1* (pCAGGS–*Hus1*) or the empty expression plasmid vector (pCAGGS-vector). Individual clones were analyzed for *Hus1* expression by RT–PCR, using primers spanning the entire *Hus1* ORF (Fig. 8A). As expected, *Hus1* expression was evident in *Hus1*$^{+/+}$*p21*$^{-/-}$ cells containing either pCAGGS-vector or pCAGGS-*Hus1. Hus1* expression was not detected in *Hus1*$^{-/-}$*p21*$^{-/-}$ clones containing pCAGGS–vector, but was restored in *Hus1*–null cells containing pCAGGS–*Hus1*. The UV sensitivity of the stable clones was then tested, and representative results are shown in Figure 8B. Clones containing pCAGGS-vector showed UV sensitivities similar to those of the parental cultures, with *Hus1*–null clones displaying increased UV sensitivity. Significantly, *Hus1* overexpression fully complemented the UV sensitivity of *Hus1*$^{-/-}$*p21*$^{-/-}$ cells, as four of four *Hus1*$^{-/-}$*p21*$^{-/-}$ clones overexpressing *Hus1* survived UV treatment as well as *Hus1*$^{+/+}$*p21*$^{-/-}$ cells (Fig. 8B; data not shown). The UV sensitivity of *Hus1*$^{+/+}$*p21*$^{-/-}$ cells was not significantly affected by *Hus1* overexpression. These results indicate that the heightened DNA damage sensitivity of *Hus1*$^{-/-}$*p21*$^{-/-}$ cells is due at least in part to the absence of *Hus1*.

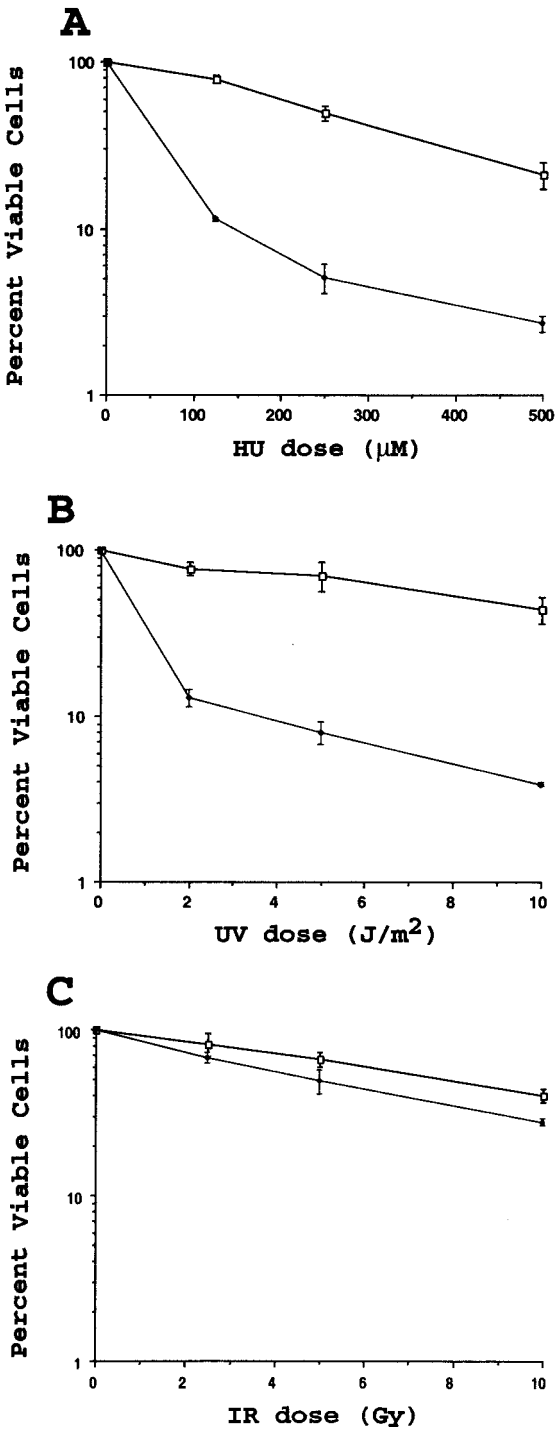

Figure 7. Increased sensitivity of *Hus1*-deficient cells to certain genotoxins. *Hus1*$^{+/+}$*p21*$^{-/-}$ (□) or *Hus1*$^{-/-}$*p21*$^{-/-}$ (♦) MEFs were plated in 6-well culture dishes and treated with the indicated doses of (*A*) HU, (*B*) UV, or (*C*) IR as described in Materials and Methods. Cell viability was assessed 72 hr after treatment and is plotted as the percent viable cells relative to results for untreated control cultures. Each point represents the mean of three samples, with error bars showing standard deviation. The plots are representative of results obtained for three independent *Hus1*$^{-/-}$*p21*$^{-/-}$ and matched control *Hus1*$^{+/+}$*p21*$^{-/-}$ MEF cultures.

Discussion

Fission yeast *hus1*$^{+}$ is a component of the cellular machinery that responds to stalled DNA replication and DNA damage. In the present study, we examined the functions of the mouse homolog of *S. pombe hus1*$^{+}$ by assessing the consequences of a targeted disruption of mouse *Hus1*. Our findings identify an important role for *Hus1* in the maintenance of genomic stability, as inactivation of *Hus1* in mouse embryos resulted in an accumulation of spontaneous genome damage, widespread

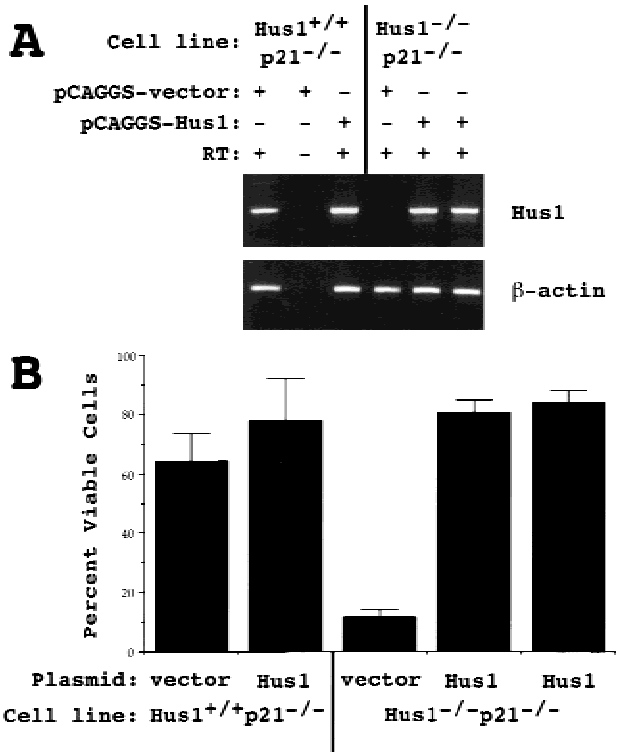

Figure 8. Restoration of *Hus1* expression complements the UV sensitivity of *Hus1*-deficient cells. $Hus1^{-/-}p21^{-/-}$ and $Hus1^{+/+}p21^{-/-}$ MEFs were stably transfected with either an empty expression plasmid vector (pCAGGS–vector) or an expression plasmid encoding *Hus1* (pCAGGS–*Hus1*). (*A*) Gene expression in individual stable clones was analyzed by RT–PCR, with primers specific for *Hus1* (*top*) or β-actin (*bottom*). (*B*) The indicated cell lines were treated with 5 J/m^2 of UV and cell viability was assessed 72 hr after treatment. Values are the mean of three samples, with error bars showing standard deviation.

cell death, and ultimately embryonic lethality. In addition, *Hus1*-null cells were found to be highly sensitive to the DNA replication inhibitor hydroxyurea and DNA damaging ultraviolet light, indicating that mouse *Hus1*, like its fission yeast counterpart, participates in cellular responses to genotoxic stress.

Mouse *Hus1* is essential for proper embryonic development, whereas fission yeast lacking $hus1^+$ appear normal under standard growth conditions (Enoch et al. 1992). This may indicate that mouse *Hus1* mediates additional functions not performed by its fission yeast homolog, or that fundamental physiological differences between yeast and mammalian cells create a greater requirement for mouse *Hus1*. Yet, *Hus1* is not absolutely required for cell survival, as $Hus1^{-/-}p21^{-/-}$ MEFs with normal growth capacities could be generated. In *Drosophila*, homologs of the fission yeast checkpoint proteins $chk1^+$ (*grapes*) and $rad3^+$ (*mei-41*) are essential specifically during embryonic development, but are dispensable in the adult fly (Hari et al. 1995; Fogarty et al. 1997; Sibon et al. 1997, 1999). Mouse embryogenesis may similarly create a strict requirement for *Hus1*. Cell division can occur as rapidly as every 2–3 hr in some regions of gastrulating mouse embryos (Snow 1977), and these extraordinary circumstances might necessitate regulatory mechanisms to ensure the correct ordering of cell cycle events or the repair of DNA damage. Conditional gene targeting should reveal the role of *Hus1* in adult tissues.

Inactivation of *Hus1* results in genomic instability, as evidenced by the increased expression of DNA damage-inducible genes in $Hus1^{-/-}$ embryos and the presence of increased chromosomal abnormalities in primary $Hus1^{-/-}$ embryo cultures. The identification of a role for *Hus1* in genome maintenance raises the possibility that *Hus1* is a tumor suppressor gene, as genetic instability may be an important driving force in tumorigenesis (Hartwell and Kastan 1994; Lengauer et al. 1998). Although it has not been determined whether human *HUS1* is mutated in any malignancies, the *HUS1* locus resides in a genomic region reported to be altered in choriocarcinomas and ovarian cancers (Dean et al. 1998).

The molecular basis for the abnormalities that arise in the absence of *Hus1* remains unknown. The chromosomal aberrations visible in metaphase spreads from $Hus1^{-/-}$ embryos, mostly chromatid breaks, are similar to those that occur in normal embryos and therefore may represent spontaneous DNA damage that would ordinarily be repaired in a *Hus1*-dependent manner. On the other hand, loss of *Hus1* may promote the occurrence of DNA damage. Premature progression of cells with incompletely-replicated chromosomes into mitosis due to the absence of a *Hus1*-mediated checkpoint could result in significant genome damage. Alternatively, the genome damage observed in *Hus1*-null cells could be the consequence of a failure to properly recover from transient S-phase arrest, as *S. pombe* $hus1^+$ plays an important role during S-phase in the response to stalled DNA replication (Enoch et al. 1992). Further analysis of the *Hus1*-deficient cells should reveal which of these possible defects is responsible for the genome damage that occurs in the absence of *Hus1*.

$Hus1^{-/-}$ embryonic fibroblasts fail to proliferate and cannot be serially passaged. However, inactivation of *p21* allowed for the continued growth of *Hus1*-deficient MEFs. The poor growth of *Atm*-null MEFs in vitro can similarly be rescued by deletion of *p21* (Wang et al. 1997; Xu et al. 1998). We suspect that genome damage in $Hus1^{-/-}$ MEFs triggers cell cycle arrest and that removal of *p21* enables the damaged cells to continue cycling. Consistent with this possibility, $Hus1^{-/-}p21^{-/-}$ MEFs proliferate despite numerous chromosomal abnormalities (data not shown). That genome damage in $Hus1^{-/-}$ embryos is accompanied by widespread apoptosis, rather than growth arrest, may be a reflection of tissue-specific DNA damage responses (for review, see Evan and Littlewood 1998; Bates and Vousden 1999). It should be noted that loss of *p21* does not allow for the survival of *Hus1*-null mice; whether it partially rescues the developmental defects of $Hus1^{-/-}$ embryos is under investigation.

$Hus1^{-/-}p21^{-/-}$ cells are highly sensitive to HU and UV, but show little increase in IR sensitivity compared

to *Hus1*$^{+/+}$*p21*$^{-/-}$ cells. Although we cannot rule out a contribution from *p21*-deficiency, these phenotypes are due at least in part to the absence of *Hus1*, as restoration of *Hus1* expression fully complements the UV sensitivity of *Hus1*$^{-/-}$*p21*$^{-/-}$ cells. These results establish a role for *Hus1* in the response to DNA replication blocks and certain forms of DNA damage. Considering that UV and IR cause different types of DNA lesions, a pathway involving *Hus1* might recognize UV photoproducts, but not strand breaks caused by IR. The *rad3*$^{+}$-related checkpoint gene *Atm* provides a precedent for such specialization in mammalian DNA damage responses. Whereas fission yeast lacking *rad3*$^{+}$ are sensitive to both IR and UV (Al-Khodairy and Carr 1992; Jimenez et al. 1992), *Atm*-deficient cells are sensitive to IR, but not UV (for review, see Rotman and Shiloh 1999). Thus, in mammalian cells *Hus1* might respond specifically to DNA damage caused by UV. Alternatively, the increased UV sensitivity of *Hus1*$^{-/-}$*p21*$^{-/-}$ cells might reflect a deficiency in an S-phase arrest response, rather than a DNA damage checkpoint defect, as most DNA polymerases are unable to replicate templates containing UV-induced DNA lesions (for review, see Naegeli 1994). Finally, although the *Hus1*$^{-/-}$*p21*$^{-/-}$ cells show only slightly increased IR sensitivity, a role for *Hus1* in responding to IR-induced DNA damage cannot be excluded. An evolutionarily conserved function for the Hus1/Rad1/Rad9 complex in responding to strand breaks is suggested by the finding that the *Caenorhabditis elegans* homolog of *S. pombe rad1*$^{+}$ (*mrt-2*) is required for IR-induced apoptosis in germ cells (Gartner et al. 2000). A similar function for mouse *Hus1* might be masked by redundant pathways that can respond to the same damage. Because primary *Hus1*$^{-/-}$ cells contain numerous chromatid breaks, it also remains possible that the *Hus1*$^{-/-}$*p21*$^{-/-}$ cells have adapted to this form of DNA damage and therefore are less sensitive to IR.

This analysis of *Hus1*-deficient embryos and cells implicates *Hus1* in a subset of mammalian checkpoint pathways. An important component of many mammalian DNA damage responses is the transcription factor *p53*, which becomes activated in response to genotoxic stress and induces the expression of genes involved in cell cycle control, apoptosis, and DNA repair (for review, see Levine 1997). *Hus1*$^{-/-}$ embryos show elevated expression of *p53* target genes *p21*, *Mdm2*, and *Bax*, and appear proficient for IR-induced apoptosis (R. Weiss and P. Leder, unpubl.), another process largely dependent on *p53* (Norimura et al. 1996). Although direct analysis of *p53* in *Hus1*-deficient cells is still necessary, these data suggest that *Hus1* may not be required for *p53* activation. In fission yeast, *hus1*$^{+}$ acts in the same pathway as *rad3*$^{+}$ (for review, see Caspari and Carr 1999). Whereas the mammalian checkpoint genes *Atm* and *Atr* are both related to *rad3*$^{+}$, several lines of evidence suggest that mouse *Hus1* acts in conjunction with *Atr*, rather than *Atm*. Like *Hus1*, *Atr* is essential, and both *Atr*$^{-/-}$ and *Hus1*$^{-/-}$ embryos show spontaneous chromosomal abnormalities and extensive apoptosis (Brown and Baltimore 2000). In contrast, *Atm* is not an essential gene (for review, see Rotman and Shiloh 1999). Furthermore, cells overexpressing dominant-negative Atr, like *Hus1*-null cells, show increased sensitivity to UV and HU (Cliby et al. 1998; Wright et al. 1998), whereas *Atm*$^{-/-}$ cells are not hypersensitive to UV or HU. Because *Atr* also appears to act in response to IR and *Atr*-null embryos die earlier in development than *Hus1*$^{-/-}$ embryos, *Atr* likely has additional *Hus1*-independent functions. The *Hus1*-deficient cells described in this study should be a useful tool for assessing the possible functional interactions between *Hus1* and *Atr*, as well as other checkpoint components. The strong links between cell cycle checkpoints and cancer prevention underscore the importance of such efforts to develop a detailed understanding of mammalian checkpoint pathways.

Materials and methods

Plasmids

A *Hus1* targeting vector was constructed in two steps in the OS.DUP/DEL vector (a gift of O. Smithies), which contains a loxP-flanked MC1-*Neo* expression cassette for positive selection and a PGK-*TK* expression module for negative selection. First, an ~4-kb *Nhe*I fragment from plasmid pMH1 (Weiss et al. 1999) was subcloned into the *Nhe*I site of OS.DUP/DEL, producing pOS–HKO5′. Next, an ~3.5-kb *Sma*I–*Eco*RV fragment was removed from plasmid pMH1, blunt-ended, and cloned into a blunt-ended *Bam*HI site of pOS–HKO5′, generating the final targeting construct, pOS–HKO (Fig. 1A). After generating *Hus1*$^{+/-}$ mice using pOS-HKO, we were notified that the *Neo* cassette in OS.DUP/DEL does not contain a polyA signal sequence (O. Smithies, pers. comm.). However, in the case of *Hus1* targeting, this did not appear to compromise *Neo* function, as evidenced by the appearance of typical numbers of G418-resistant colonies (data not shown), or lead to the generation of detectable read-through transcripts in embryos (see Fig. 5A). The *Hus1* expression plasmid pCAGGS–*Hus1* was generated by cloning the *Hus1* ORF into the pCAGGS vector (Niwa et al. 1991).

ES cell culture, gene targeting, and generation of Hus1 *mice*

TC-1 ES cells were electroporated with *Not*I-linearized pOS-HKO and selected in G418 and FIAU as described previously (Deng et al. 1996). Genomic DNA from 120 drug-resistant colonies was screened for homologous recombination at the *Hus1* locus by Southern blot hybridization with an external probe, and eight correctly-targeted clones were identified. The correct targeting of the heterozygous clones was verified by additional Southern blot analyses using alternative restriction enzyme digests, as well as an internal probe. ES cells from correctly-targeted clones were micro-injected into C57BL/6 (Taconic) blastocysts, which were then transferred into pseudopregnant Swiss Webster (Taconic) foster mothers. Chimeric male mice, identified by the presence of agouti coat color, were mated to 129S6 (Taconic) and Black Swiss (Taconic) females, and transmission of the targeted allele through the germline was determined by coat color and Southern blot analyses. Mice heterozygous for the targeted allele were intercrossed and also mated to EIIa-*cre* transgenic mice (a gift of F. Alt) for *cre*-mediated recombination and excision of the *Neo* cassette (Lakso et al. 1996). For timed matings, mice were mated overnight and females were in-

spected for vaginal plugs the following morning. Noon on the day of vaginal plug detection was defined as day 0.5 of gestation.

Genotyping by Southern blot and PCR analyses

Genomic DNA was isolated from ES cells and tail biopsy fragments by proteinase K digestion and precipitation with ethanol. Whole-embryo and yolk sac genomic DNA was prepared by incubating samples in digestion buffer (500 mM Tris at pH 9.5, 10 mM NaCl, 20 mM EDTA, 3.0% Tween-20, 0.5% xylene cyanol, 1.5 mg/ml proteinase K) at 50°C overnight, diluting the sample fivefold with water, and heating at 100°C for 10 min. Genomic DNA was obtained from embryo sections as described (Zeitlin et al. 1995). For Southern blot analyses, approximately 10 μg of genomic DNA was digested with *Bgl*I, resolved on a 0.8% agarose gel, transferred to a nylon membrane, and hybridized with ^{32}P-labeled probe. To generate an external probe, we first subcloned a blunt-ended *Bgl*I–*Bam*HI fragment from plasmid pMH2 (Weiss et al. 1999) into the *Sma*I site of pBluescript-SK, producing pBS–Int4. The flanking probe (Fig. 1A) was a *Ssp*I–*Pst*I fragment from pBS–Int4. For PCR analysis, 0.5–2.0 μl of genomic DNA was PCR amplified with Taq DNA polymerase (Boehringer Mannheim) under standard reaction conditions in a total volume of 50 μl with the three oligonucleotide primers depicted in Figure 1A: (a) 5′-CCGTCGGCCTGGTATCCGCCATGA-3′; (b) 5′-GGTATCGCCGCTCCCGATTCGCAG-3′; (c) 5′-GGGCTGATGCGGAGGGTGCAGGTT-3′. After denaturation at 94°C for 5 min, 35 cycles of amplification (94°C, 20 sec; 60°C, 30 sec; 72°C, 1 min) were performed, followed by a final extension step of 72°C for 10 min.

Histological analyses

Decidua from timed *Hus1* heterozygote matings were isolated at 7.5–9.5 dpc. Following fixation for 2–4 hr at 4°C in 4% paraformaldehyde, 1× PBS (137 mM NaCl, 2.7 mM KCl, 4.3 mM Na_2HPO_4, 1.4 mM KH_2PO_4), decidua were sequentially dehydrated in 50%, 70%, 95%, and 100% ethanol, cleared in xylenes, and embedded in paraffin. Paraffin blocks were sectioned at 5 μm. Staining of sections by the Feulgen reaction was performed as described previously (Chester et al. 1998). TUNEL staining was performed with the ApopTag peroxidase in Situ apoptosis detection kit (Intergen Co.) according to the manufacturer's directions. VIP (Vector Laboratories) was used as the peroxidase substrate, and counterstaining was performed with 0.5% (wt/vol) methyl green in 0.1 M sodium acetate (pH 4.0). To analyze BrdU incorporation, we injected BrdU (100 μg per gram of body weight) intraperitoneally into pregnant females. One hour after BrdU injection, decidua were isolated, processed, and sectioned as described above. BrdU staining was performed with a biotinylated mouse anti-BrdU antibody using a BrdU staining kit (Zymed Laboratories, Inc.) according to the manufacturer's directions, with the exception that 5 μg/ml proteinase K was used in place of trypsin for antigen retrieval. DAB was used as the peroxidase substrate and counterstaining was performed with hematoxylin.

Northern blot hybridizations and RT–PCR

Embryos from timed *Hus1* heterozygote matings at 8.5 dpc were dissected free of the decidua. Total RNA was prepared from individual embryos, including yolk sac and amnion, or MEF cultures using the RNA STAT-60 reagent (Tel-Test, Inc.). A fraction of each RNA sample was reserved for genotyping by PCR and the remainder was subjected to Northern blotting as described previously (Weiss et al. 1999). For RT–PCR, cDNA was prepared from 5 μg of DNase-treated total RNA by random priming using the SuperScript preamplification system (Life Technologies, Inc.). PCR amplification of cDNAs was done using primers specific for *Hus1* (5′-ATGAAGTTTCGCGCCAAGATCGTGGACC-3′ and 5′-CTAGGACAAGGCTGGGATGAAATACTG-3′) or β-actin (5′-TGTGATGGTGGGAATGGGTCAG-3′ and 5′-TTTGATGTCACGCACGATTTCC-3′).

Chromosome preparations

Embryos from *Hus1* heterozygote intercrosses at 9.5 dpc were dissected from the deciduum in Hanks' Balanced Salt Solution, mechanically disrupted in 100 μl of 0.25% trypsin, 1.0 mM EDTA, and placed into individual wells of gelatinized 24-well culture dishes in culture medium (DMEM supplemented with 20% fetal bovine serum, 1.0 mM L-glutamine, 0.1 mM MEM non-essential amino acids, 100 μg/ml of streptomycin sulfate, and 100 U/ml of penicillin). Yolk sacs were reserved for genotyping. The following day, the embryo cultures were incubated in culture medium containing 0.1 μg/ml of colcemid for 2 hr. Cells were then harvested by trypsinization, swollen for 10 min at 37°C in 0.075 M KCl, and fixed for at least 20 min at 4°C in 75% methanol, 25% acetic acid. Cells in fixative were then spotted onto microscope slides and stained with 2.0% Giemsa in phosphate buffer (pH 6.8). Chromosomal abnormalities were scored based on guidelines in the International System for Human Cytogenetic Nomenclature (Mitelman 1995). Statistical comparison of the frequency of chromosomal abnormalities was done by Pearson Chi-square.

Hus1 *MEF cultures, cell survival assays, and stable transfections*

Hus1$^{+/-}$ mice were bred with *p21*$^{-/-}$ mice (Deng et al. 1995), and individual embryos from *Hus1*$^{+/-}$*p21*$^{-/-}$ intercrosses at 9.5 dpc were placed into culture as described above. After the cultures expanded to fill a 10-cm dish, the culture medium serum content was reduced to 10%, and the cells were subsequently maintained on a 3T3 culture protocol in which 10^6 cells were passed onto a new gelatinized 10-cm dish every three days. Sensitivity to genotoxins was assessed by seeding 10^5 cells into individual gelatinized wells of a six-well dish in triplicate and treating the cultures the following day. For UV treatment, the culture medium was removed, cells were exposed to 254 nm UV light in a XL-1500 Spectrolinker (Spectronics Corp), and fresh medium was placed onto the cells. For IR treatment, cells were irradiated with a ^{137}Cs source (Mark 1 Irradiator, J.L. Sheperd and Sons) at a dose rate of 2.0 Gy/min. For HU treatment, cells were cultured in medium containing HU (Sigma) for 24 hr, and then the medium was removed and replaced with culture medium lacking HU. Three days after treatment, cells were harvested by trypsinization, incubated with trypan blue dye, and counted. For restoration of *Hus1* expression, MEFs were transfected with either 2.0 μg pCAGGS-vector or 2.0 μg of pCAGGS-*Hus1* and 0.2 μg of PGK-puro DNA using the Lipofectamine Plus transfection reagent (Life Technologies, Inc.) according to manufacturer's directions. Transfected cells were selected in 2.5 μg/ml of puromycin, and individual clones were isolated, expanded, and analyzed.

Acknowledgments

We thank Fred Alt, Nick Chester, Jan Pinkas, and Oliver Smithies for reagents; Cynthia Morton and Charles Lee for advice on

chromosome analysis; Anne Harrington for performing blastocyst microinjections; Cathie Daugherty for assistance with ES cell culture; Rick Van Etten for assistance with cell irradiation; and Mark Bedford, Nick Chester, Liz Harrington, Boris Reizis, Yaoqi Wang, and Tom Wolkow for helpful discussions and for critically reading the manuscript. R.S.W. is supported by a postdoctoral fellowship (PF-98-131-01) from the American Cancer Society, T.E. is supported by NIH grant number GM50015, and P.L. is a senior investigator of the Howard Hughes Medical Institute.

The publication costs of this article were defrayed in part by payment of page charges. This article must therefore be hereby marked "advertisement" in accordance with 18 USC section 1734 solely to indicate this fact.

References

Ahmed, S. and Hodgkin, J. 2000. MRT-2 checkpoint protein is required for germline immortality and telomere replication in *C. elegans. Nature* **403:** 159–164.

Al-Khodairy, F. and Carr, A.M. 1992. DNA repair mutants defining G2 checkpoint pathways in *Schizosaccharomyces pombe. EMBO J.* **11:** 1343–1350.

Al-Khodairy, F., Fotou, E., Sheldrick, K.S., Griffiths, D.J., Lehmann, A.R., and Carr, A.M. 1994. Identification and characterization of new elements involved in checkpoint and feedback controls in fission yeast. *Mol. Biol. Cell* **5:** 147–160.

Aravind, L., Walker, D.R., and Koonin, E.V. 1999. Conserved domains in DNA repair proteins and evolution of repair systems. *Nucleic Acids Res.* **27:** 1223–1242.

Bates, S. and Vousden, K.H. 1999. Mechanisms of p53-mediated apoptosis. *Cell. Mol. Life Sci.* **55:** 28–37.

Bell, D.W., Varley, J.M., Szydlo, T.E., Kang, D.H., Wahrer, D.C., Shannon, K.E., Lubratovich, M., Verselis, S.J., Isselbacher, K.J., Fraumeni, J.F., et al. 1999. Heterozygous germ line *hCHK2* mutations in Li-Fraumeni syndrome. *Science* **286:** 2528–2531.

Brown, E.J. and Baltimore, D. 2000. *ATR* disruption leads to chromosomal fragmentation and early embryonic lethality. *Genes & Dev.* **14:** 397–402.

Caspari, T. and Carr, A.M. 1999. DNA structure checkpoint pathways in *Schizosaccharomyces pombe. Biochimie* **81:** 173–181.

Caspari, T., Dahlen, M., Kanter-Smoler, G., Lindsay, H.D., Hofmann, K., Papadimitriou, K., Sunnerhagen, P., and Carr, A.M. 2000. Characterization of *Schizosaccharomyces pombe* Hus1: A PCNA-related protein that associates with Rad1 and Rad9. *Mol. Cell. Biol.* **20:** 1254–1262.

Chester, N., Kuo, F., Kozak, C., O'Hara, C.D., and Leder, P. 1998. Stage-specific apoptosis, developmental delay, and embryonic lethality in mice homozygous for a targeted disruption in the murine Bloom's syndrome gene. *Genes & Dev.* **12:** 3382–3393.

Cliby, W.A., Roberts, C.J., Cimprich, K.A., Stringer, C.M., Lamb, J.R., Schreiber, S.L., and Friend, S.H. 1998. Overexpression of a kinase-inactive ATR protein causes sensitivity to DNA-damaging agents and defects in cell cycle checkpoints. *EMBO J.* **17:** 159–169.

Copp, A.J. 1995. Death before birth: Clues from gene knockouts and mutations. *Trends Genet.* **11:** 87–93.

Cross, J.C., Werb, Z., and Fisher, S.J. 1994. Implantation and the placenta: Key pieces of the development puzzle. *Science* **266:** 1508–1518.

Dahlen, M., Olsson, T., Kanter-Smoler, G., Ramne, A., and Sunnerhagen, P. 1998. Regulation of telomere length by checkpoint genes in *Schizosaccharomyces pombe. Mol. Biol. Cell* **9:** 611–621.

Dasika, G.K., Lin, S.C., Zhao, S., Sung, P., Tomkinson, A., and Lee, E.Y. 1999. DNA damage-induced cell cycle checkpoints and DNA strand break repair in development and tumorigenesis. *Oncogene* **18:** 7883–7899.

Dean, F.B., Lian, L., and O'Donnell, M. 1998. cDNA cloning and gene mapping of human homologs for *Schizosaccharomyces pombe rad17*, *rad1*, and *hus1* and cloning of homologs from mouse, *Caenorhabditis elegans*, and *Drosophila melanogaster. Genomics* **54:** 424–436.

Deng, C., Zhang, P., Harper, J.W., Elledge, S.J., and Leder, P. 1995. Mice lacking $p21^{CIP1/WAF1}$ undergo normal development, but are defective in G1 checkpoint control. *Cell* **82:** 675–684.

Deng, C., Wynshaw-Boris, A., Zhou, F., Kuo, A., and Leder, P. 1996. Fibroblast growth factor receptor 3 is a negative regulator of bone growth. *Cell* **84:** 911–921.

Desany, B.A., Alcasabas, A.A., Bachant, J.B., and Elledge, S.J. 1998. Recovery from DNA replicational stress is the essential function of the S-phase checkpoint pathway. *Genes & Dev.* **12:** 2956–2970.

Elledge, S.J. 1996. Cell cycle checkpoints: Preventing an identity crisis. *Science* **274:** 1664–1672.

Enoch, T., Carr, A.M., and Nurse, P. 1992. Fission yeast genes involved in coupling mitosis to completion of DNA replication. *Genes & Dev.* **6:** 2035–2046.

Evan, G. and Littlewood, T. 1998. A matter of life and cell death. *Science* **281:** 1317–1322.

Fogarty, P., Campbell, S.D., Abu-Shumays, R., Phalle, B.S., Yu, K.R., Uy, G.L., Goldberg, M.L., and Sullivan, W. 1997. The *Drosophila grapes* gene is related to checkpoint gene *chk1/rad27* and is required for late syncytial division fidelity. *Curr. Biol.* **7:** 418–426.

Freire, R., Murguia, J.R., Tarsounas, M., Lowndes, N.F., Moens, P.B., and Jackson, S.P. 1998. Human and mouse homologs of *Schizosaccharomyces pombe rad1*$^+$ and *Saccharomyces cerevisiae RAD17*: Linkage to checkpoint control and mammalian meiosis. *Genes & Dev.* **12:** 2560–2573.

Gartner, A., Milstein, S., Ahmed, S., Hodgkin, J., and Hengartner, M.O. 2000. A conserved checkpoint pathway mediates DNA damage-induced apoptosis and cell cycle arrest in *C. elegans. Mol. Cell* **5:** 435–443.

Hari, K.L., Santerre, A., Sekelsky, J.J., McKim, K.S., Boyd, J.B., and Hawley, R.S. 1995. The *mei-41* gene of D. melanogaster is a structural and functional homolog of the human ataxia telangiectasia gene. *Cell* **82:** 815–821.

Hartwell, L.H. and Kastan, M.B. 1994. Cell cycle control and cancer. *Science* **266:** 1821–1828.

Hartwell, L.H. and Weinert, T.A. 1989. Checkpoints: Controls that ensure the order of cell cycle events. *Science* **246:** 629–634.

Hollander, M.C., Zhan, Q., Bae, I., and Fornace Jr, A.J. 1997. Mammalian *GADD34*, an apoptosis- and DNA damage-inducible gene. *J. Biol. Chem.* **272:** 13731–13737.

Jimenez, G., Yucel, J., Rowley, R., and Subramani, S. 1992. The *rad3*$^+$ gene of *Schizosaccharomyces pombe* is involved in multiple checkpoint functions and in DNA repair. *Proc. Natl. Acad. Sci.* **89:** 4952–4956.

Ko, L.J. and Prives, C. 1996. p53: Puzzle and paradigm. *Genes & Dev.* **10:** 1054–1072.

Kostrub, C.F., Al-Khodairy, F., Ghazizadeh, H., Carr, A.M., and Enoch, T. 1997. Molecular analysis of *hus1*$^+$, a fission yeast gene required for S-M and DNA damage checkpoints. *Mol. Gen. Genet.* **254:** 389–399.

Kostrub, C.F., Knudsen, K., Subramani, S., and Enoch, T. 1998. Hus1p, a conserved fission yeast checkpoint protein, interacts with Rad1p and is phosphorylated in response to DNA damage. *EMBO J.* **17:** 2055–2066.

Kuznetsova, M.N. 1957. Histopathology of the placenta in radiation sickness. *Akush. Ginekol. (Mosc.)* **33/4:** 50–55.

Lakso, M., Pichel, J.G., Gorman, J.R., Sauer, B., Okamoto, Y., Lee, E., Alt, F.W., and Westphal, H. 1996. Efficient *in vivo* manipulation of mouse genomic sequences at the zygote stage. *Proc. Natl. Acad. Sci.* **93:** 5860–5865.

Lengauer, C., Kinzler, K.W., and Vogelstein, B. 1998. Genetic instabilities in human cancers. *Nature* **396:** 643–649.

Levine, A.J. 1997. p53, the cellular gatekeeper for growth and division. *Cell* **88:** 323–331.

Mitelman, F. 1995. *ISCN (1995): An International System for Human Cytogenetic Nomenclature.* S. Karger, Basel.

Naegeli, H. 1994. Roadblocks and detours during DNA replication: Mechanisms of mutagenesis in mammalian cells. *BioEssays* **16:** 557–564.

Niwa, H., Yamamura, K., and Miyazaki, J. 1991. Efficient selection for high-expression transfectants with a novel eukaryotic vector. *Gene* **108:** 193–199.

Norimura, T., Nomoto, S., Katsuki, M., Gondo, Y., and Kondo, S. 1996. *p53*-dependent apoptosis suppresses radiation-induced teratogenesis. *Nat. Med.* **2:** 577–580.

Page, A.W. and Orr-Weaver, T.L. 1997. Stopping and starting the meiotic cell cycle. *Curr. Opin. Genet. Dev.* **7:** 23–31.

Parker, A.E., Van de Weyer, I., Laus, M.C., Oostveen, I., Yon, J., Verhasselt, P., and Luyten, W.H. 1998. A human homologue of the *Schizosaccharomyces pombe rad1*$^+$ checkpoint gene encodes an exonuclease. *J. Biol. Chem.* **273:** 18332–18339.

Rinkenberger, J.L., Cross, J.C., and Werb, Z. 1997. Molecular genetics of implantation in the mouse. *Dev. Genet.* **21:** 6–20.

Rotman, G. and Shiloh, Y. 1999. ATM: A mediator of multiple responses to genotoxic stress. *Oncogene* **18:** 6135–6144.

Rowley, R., Subramani, S., and Young, P.G. 1992. Checkpoint controls in *Schizosaccharomyces pombe*: *rad1. EMBO J.* **11:** 1335–1342.

Sibon, O.C., Laurencon, A., Hawley, R., and Theurkauf, W.E. 1999. The *Drosophila* ATM homologue Mei-41 has an essential checkpoint function at the midblastula transition. *Curr. Biol.* **9:** 302–312.

Sibon, O.C., Stevenson, V.A., and Theurkauf, W.E. 1997. DNA-replication checkpoint control at the *Drosophila* midblastula transition. *Nature* **388:** 93–97.

Snow, M.H.L. 1977. Gastrulation in the mouse: Growth and regionalization of the epiblast. *J. Embryol. Exp. Morph.* **42:** 293–303.

St. Onge, R.P., Udell, C.M., Casselman, R., and Davey, S. 1999. The human G2 checkpoint control protein hRAD9 is a nuclear phosphoprotein that forms complexes with hRAD1 and hHUS1. *Mol. Biol. Cell* **10:** 1985–1995.

Volkmer, E. and Karnitz, L.M. 1999. Human homologs of *Schizosaccharomyces pombe Rad1*, *Hus1*, and *Rad9* form a DNA damage-responsive protein complex. *J. Biol. Chem.* **274:** 567–570.

Walshtrem, E.A. 1960. Pathogenesis of irradiation hazards and reparative processes in rat embryos after x-raying of rat females on the 10th day of pregnancy. *Arkh. Anat. Gistol. Embriol.* **38:** 72–79.

Wang, Y.A., Elson, A., and Leder, P. 1997. Loss of *p21* increases sensitivity to ionizing radiation and delays the onset of lymphoma in *atm*-deficient mice. *Proc. Natl. Acad. Sci.* **94:** 14590–14595.

Weiss, R.S., Kostrub, C.F., Enoch, T., and Leder, P. 1999. Mouse *Hus1*, a homolog of the *Schizosaccharomyces pombe hus1*$^+$ cell cycle checkpoint gene. *Genomics* **59:** 32–39.

Wright, J.A., Keegan, K.S., Herendeen, D.R., Bentley, N.J., Carr, A.M., Hoekstra, M.F., and Concannon, P. 1998. Protein kinase mutants of human ATR increase sensitivity to UV and ionizing radiation and abrogate cell cycle checkpoint control. *Proc. Natl. Acad. Sci.* **95:** 7445–7450.

Xu, Y., Yang, E.M., Brugarolas, J., Jacks, T., and Baltimore, D. 1998. Involvement of p53 and p21 in cellular defects and tumorigenesis in Atm$^{-/-}$ mice. *Mol. Cell. Biol.* **18:** 4385–4390.

Zeitlin, S., Liu, J.P., Chapman, D.L., Papaioannou, V.E., and Efstratiadis, A. 1995. Increased apoptosis and early embryonic lethality in mice nullizygous for the Huntington's disease gene homologue. *Nat. Genet.* **11:** 155–163.

Zhao, X., Muller, E.G., and Rothstein, R. 1998. A suppressor of two essential checkpoint genes identifies a novel protein that negatively affects dNTP pools. *Mol. Cell* **2:** 329–340.